AIAA AVIATION FORUM AND ASCEND 2024
29 July - 2 August 2024, Las Vegas, Nevada
AIAA 2024-3773
DOI: 10.2514/6.2024-3773

Case Studies in Modelling Cruise-generated Trailing Vortices

Anthony P Brown[1]
[1]*National Research Council Canada (NRC), Flight Research Laboratory, U-61 Uplands, Ottawa, Ontario, K1A0R6, Canada*

Frank Holzäpfel[2]
[2]*Deutsches Zentrum für Luft- und Raumfahrt, Institut für Physik der Atmosphäre, 82234 Oberpfaffenhofen, Germany*

Trailing vortices from jet transport aircraft in high altitude cruising flight, have been measured in high spatiotemporal detail, by an NRC research jet. The vortex locations, descent rate and vortex core thermodynamic, dynamic, transport and spatial scale characteristics were derived. Also, from these measurements, the background atmospheric state properties of pressure, wind structure, temperature, potential temperature, thermal stratification and turbulence have been established. Thereafter, two versions of the Probabilistic 2-Phase wake vortex prediction model P2P have been applied to the cases. While the established P2P version uses ground-based measurement data to calibrate its probabilistic envelopes, the runtime optimized airborne version P2P^a uses uncertainties of all relevant impact parameters to construct the probabilistic envelopes. Flight and model data have been compared and the suitability of the P2P models for onboard wake vortex prediction and warning during cruise have been discussed.

Nomenclature

b	=	geometric wingspan of the wake generator
b_V	=	trailing pair vortex separation, lateral separation between centres (m)
DLR	=	Deutsches Zentrum für Luft- und Raumfahrt (German Aerospace Center)
g	=	gravitational acceleration
h	=	height of trailing vortex generating aircraft, in the range of 11-12 km
LES	=	large eddy simulation of the Navier Stokes equations of fluid flow
M	=	Mach Number (the quotient of true airspeed and the speed of sound)
N	=	Brunt-Väisälä frequency
NRC	=	National Research Council Canada
PA	=	pressure altitude (feet)
Δp	=	flow angle surface pressure differential across two static holes, subtended asymmetrically by 50˚
q	=	turbulence velocity
r_C	=	vortex core radius, defined as the distance from vortex centre to peak tangential velocity
s	=	spanwise load factor
t	=	time (sec)
t_0	=	characteristic wake vortex timescale
T	=	temperature (K)
V_G	=	true airspeed of the wake generating aircraft (m/s)
V_θ or V_T	=	vortex induced tangential velocity magnitude, also V_T used (m/s)
W	=	weight of the trailing vortex generating aircraft (N)
WVE	=	wake vortex encounter, the intersection of an aircraft flightpath with a trailing vortex core
u	=	headwind speed (m/s)
v	=	crosswind speed (m/s)
w_0	=	initial trailing vortex descent speed
y	=	lateral displacement coordinate (m)

[1] Research Pilot Engineer, CT-133 Facility Manager, Atmospheric Research Group, SMAIAA
[2] Senior Scientist, Applied Meteorology, Associate Fellow AIAA

z = vertical displacement coordinate (m)

ε = energy dissipation rate (EDR, $m^{2/3}/s$)
Γ = trailing vortex circulation (m^2/s)
ρ = atmospheric air density (kg/m^3)

* = normalized quantity

I. Introduction

The NRC has measured the dynamic, thermodynamic, and spatiotemporal characteristics, including vertical and lateral transport, of trailing vortices, generated by heavy jet transport aircraft, undertaking cruising flight [1]. The DLR has applied two versions of its Probabilistic 2-Phase wake vortex prediction model P2P to the flight measurement data. The P2P models predict probabilistic envelopes of wake vortex transport and decay. The established P2P version is based upon analytical considerations, the adjustment to results of large eddy simulations (LES) of different research groups, and calibration with field experiment data. The airborne version P2P^a minimizes the computational effort and uses the uncertainties of the relevant input parameters to derive the probabilistic envelopes.

To the authors' knowledge there are almost no publications presenting a detailed discussion of the prediction skills of fast-time wake vortex models in cruise conditions. Most published validation work of such models to date, used data taken in the atmospheric boundary layer at low flight levels. Few exceptions are the flight tests of DLR's wake encounter avoidance and advisory system (WEAA) using P2P^a and the P2P simulations conducted in the framework of the unprecedented A388 test program [2], accomplished to determine appropriate separation standards for the A388 in the time frame from May 2005 to December 2007. Unfortunately, the latter P2P validations had to be treated as confidential and could not be published. So, in that respect the current paper fills a relevant gap demonstrating the prediction skills of two versions of fast-time wake vortex models under cruise conditions.

Three case studies comparing flight and model output data are compared. The case studies were an A388, on the 15th March 2012, an A359, on the 14th January 2019 and a DC-8, on the 8th May 2014. The impact of the input parameters on the wake vortex prediction quality and the connected limitations for operational applications is discussed.

II. Experimental details

The NRC measurement aircraft (Fig. 1) was fitted with 600 Hz inertial and airdata sampling, processing and recording. 2 cm diameter cylinders with boundary layer transition-fixing strips were installed for the instantaneous measurement of surface-flow, used for the derivation of vortex-induced flow angles. For this, differential surface pressure measurement was employed, using high-rate differential pressure transducers, sensing surface Δp across two tiny static holes, separated by an offset subtended angle of 50˚ across the cylinder surface. In the vortex crossplane (plane orthogonal to the trailing vortex axis), 600 Hz sampling resulted in a Nyquist spatial scale of a few centimetres. Inertial data was sensed by an adjacent inertial measurement unit (IMU) in the nosebay. Vectorial differencing of the true airspeed vector (transformed through Euler angles, to the earth axis system) and inertial vector resulted in the derivation of the instantaneous wind vector. Extraction of the mean wind resulted in the derivation of the vortex-induced airflow velocity.

Figure 1 NRC CT-133 research aircraft, used for trailing vortex flight research; the underwing instrumentation pods (*left*) were installed for the A359 flight data, but not for the A388 measurements on 15th March 2012. The close-up view of the airdata noseboom(*right*) highlighted, in addition to pitot-static tube, the usage of cylinders in crossflow surface pressure measurements, for flow angle derivation, due to their highly responsive aerodynamic bandwidth.

Flight profiles consisted of air traffic control vectored interceptions of Heavy Category jet transport aircraft flying enroute at heights of 10-12 km, in vortex condensate conditions (vortex core condensate, Figs. 2/3 prevailed as far as vortex lengths of 30-40 km, Fig. 3). Wake vortex projects 2006-2021 generally employed vortex core penetrations from below, *i.e.* six o'clock position, Figs. 2*right*/3 *right*. By this technique, the greatest amount of individual trailing vortex core state characteristic data was obtained, from which dynamic instability states have been obtained. From this entry position, it was possible to remain in vortex cores for times intervals of 0.6-1.2 second duration.

Figure 2 A359, 14th January 2019 intercept at 5 km distance (*left*), and amongst the trailing vortex pair, at 15 km distance (*right*)

Figure 3 A388 intercept at 3 km (*left*), apparent curvature is a camera focal length effect; amongst the vortices at ≈20 km (*right*), in asymmetric state: port vortex core seemingly burst, starboard vortex core, wavy, with helical condensate surrounding.

III. The Probabilistic Two-Phase Wake Vortex Model Versions P2P and P2P[a]

The Probabilistic Two-Phase wake vortex (WV) decay and transport model (P2P) was developed, in the first instance, to guide the safe readjustment of aircraft separations during approach and landing. Later it was also applied successfully to departures and cruise. For this purpose, such a real-time model must be capable of reliably and quickly predicting vortex positions and strengths. P2P considers all effects of the leading order impact parameters: aircraft configuration (span, weight, speed, heading, flight path angle), as well as the environmental parameters of wind (cross and head components), wind shear, turbulence, temperature stratification, and proximity of the ground. The model predicts the deterministic (mean) evolution (D2P model), together with envelopes for vortex trajectories and strengths, with specified probabilities (P2P model). The model design rests on four pillars: dimensional analysis, the equation for the laminar decaying potential vortex, the adjustment to LES results of different groups, and the calibration with field experiment data. The design, applications, and validation activities of P2P are described in detail in a series of Journal publications [2-6]. The field experiment data used for model calibration was gathered during measurement campaigns conducted at airport [5] where both aircraft parameters and meteorological parameters can be captured

with significantly higher accuracy than at cruise altitudes. So, it is expected that the probabilistic envelopes will not be sufficiently wide for the current application of cruise flight.

The airborne model version P2P^a was tailored to the requirements of real-time airborne wake vortex prediction [7]. For this purpose, the dynamical core of the Probabilistic Two-Phase wake vortex model P2P has been retained. P2P^a focuses the modelling effort and the related computation effort on the most important impact parameters identified in a previous sensitivity study [8]. The model design distinguishes between (i) the parameters that can be modelled by the superposition of the variances of the uncertainties of the input parameters and (ii) the parameters that can only be considered via the non-linear model equations. The former approach (i) refers to the spreading of the envelopes of wake vortex position caused by uncertainties of wind, wind shear, turbulence, aircraft position, and ground altitude. The latter approach (ii) considers the effects on both vortex decay and vortex transport which are affected by the parameters that define initial circulation (mass, speed, vortex span, air density), wingspan, turbulence and temperature stratification. Off-line Monte Carlo simulations are used to adapt the probabilistic model output to envelopes of 90%, 95%, and 99% probabilities. For a prescribed probability level, this allows a reduction of internal model iterations to four by employing four dedicated combinations of the parameters: initial vortex separation, b_{V0}, initial vortex circulation, Γ_0, Brunt-Väisälä frequency, N, energy dissipation rate, ε, onset time of rapid vortex decay, T_2^*, and kinematic viscosity during rapid vortex decay, ν_2^*. These four runs yield minimum wake vortex descent distance, z_{min}, maximum vortex descent distance, z_{max}, minimum vortex lifetime, t_{min}, and maximum vortex lifetime, t_{max}.

IV. Results and Discussion

Background atmospheric data is required as state input data to the P2P models, consisting of 3-D winds, thermal stratification, and turbulence dissipation rate against pressure altitude.

A. A388 case, flight data

1. Stratification and turbulence

In presenting this data herein, the trailing vortex data is embedded in the property soundings, presenting a visual comparison of the flowfields. Fig. 4 presents flight data soundings of stratification and turbulence.

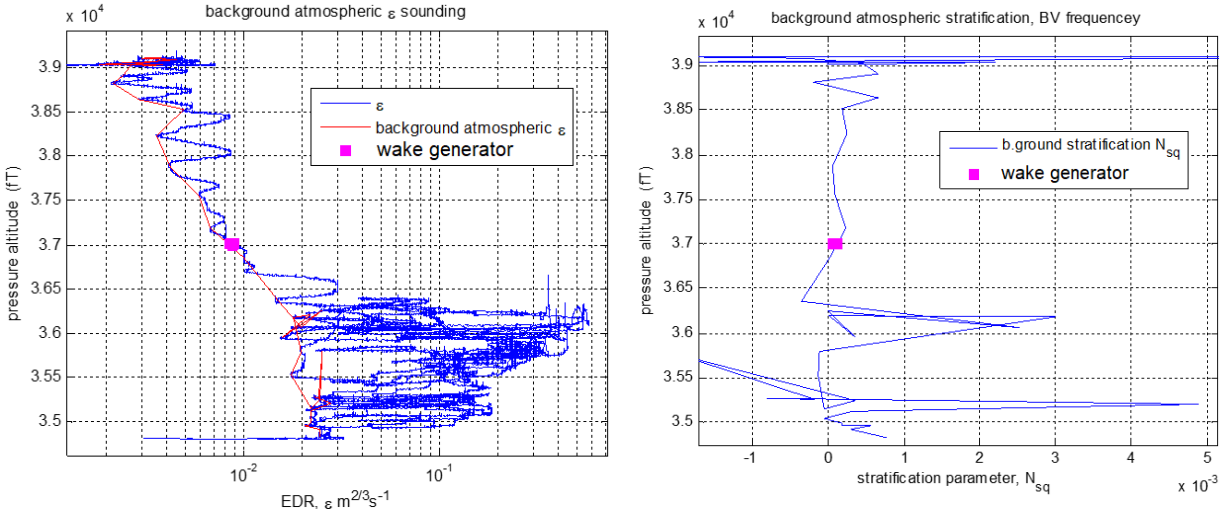

Figure 4 Eddy dissipation rate (*left*), background (0.0086 m$^{2/3}$/s at generator height) and wake vortex, and stratification (*right*), neutral at generator height.

2. Pressure, temperature and winds

The soundings of P, T and winds are presented in Fig. 5, together with the perturbations upon these quantities, induced by the trailing vortex pair. It is seen that, windspeed was reasonably constant, but backed in direction to the north with increasing height. Typical vortex-induced perturbation velocities were of the order of 20 m/s. The wake vortices were typically warmer than background, by as much as 3 K. The A388 was flying 600 m below the onset of the tropopause. In the wake vortex cores, pressure reductions of 0.5-0.7 kPa were measured.

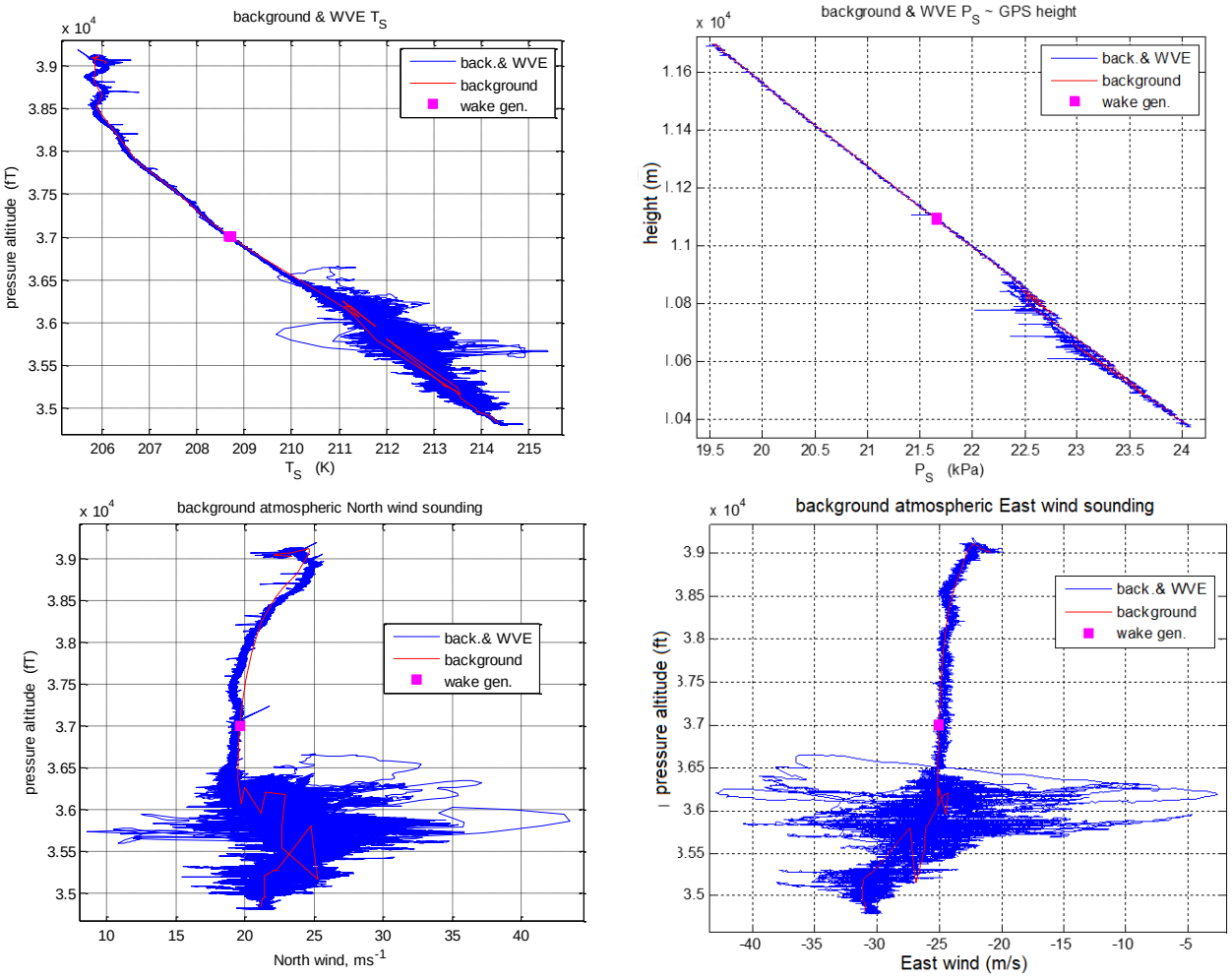

Figure 5 in-situ atmospheric soundings: (*top row*), air temperature (*left*), showing tropopause at 38,500 ft PA and vortex temperature variations of +3.5K/-1K; air pressure (*right*), showing vortex induced expansions of -0.7 kPa; (*bottom row*), north and east wind components, showing vortex-induced effects of maximum ±35 m/s.

3. Flight data of vortex generation and transport

At vortex generation altitude, atmospheric conditions were air temperature 214.8 K, air pressure 21.665 kPa (at PA of 37,000 feet) and air density 0.3617 kg/m^3. The A388 mass was 495010 kg and flying at 0.86 M, equating to 252 ms^{-1}. Derived optically *via* perspective analysis of video records similar to Figs. 2 *left*/3 *left* (but directly in-trail, thereby negating the optical curvature), b_{V0} = 52.7 m (or 65.8% of geometric span). This lateral spacing was similar to that encountered in-situ, during vortex core traverses, a number of which were concatenated for a vortex-velocity perturbation crossplane perspective, Fig. 6. By calculation, at measured b_{Vo}, vortex circulation was Γ=1,011 m^{2}s^{-1}. This data was used for the P2P initializations.

Trailing vortex transport is depicted in Fig. 7. Concerning vertical transport, the first vortex core traverse was conducted at a wake length near 10 km (approximately 45 sec age, non-dimensional wake time $t^* \approx 2.6$). For modelling vortex descent, the accuracy of the vortex generation height must be considered, which for a PA of 37,000 feet, will vary with the temperature profile of the atmosphere.

During the trailing vortex intercept descent (between 12-17 km wake length), the GPS-referenced height of a PA of 37,000 feet was measured by the CT-133, as 11.091±0.023 km. However, the height accuracy of the generator aircraft was unknown. It can be bounded by the RVSM 95% confidence tolerance of ±85.7 m. This bias error on wake generator height would track through the P2P solution; albeit an initializing error, rather than a solution confidence limit.

Each vortex core traverse defines the vertical position of the vortex core at that position. It is seen that the vertical path was generally non-linear, but varied harmonically, with variable amplitude and period. The non-linear amplitude was greatest between 35 and 45 km trailing vortex length.

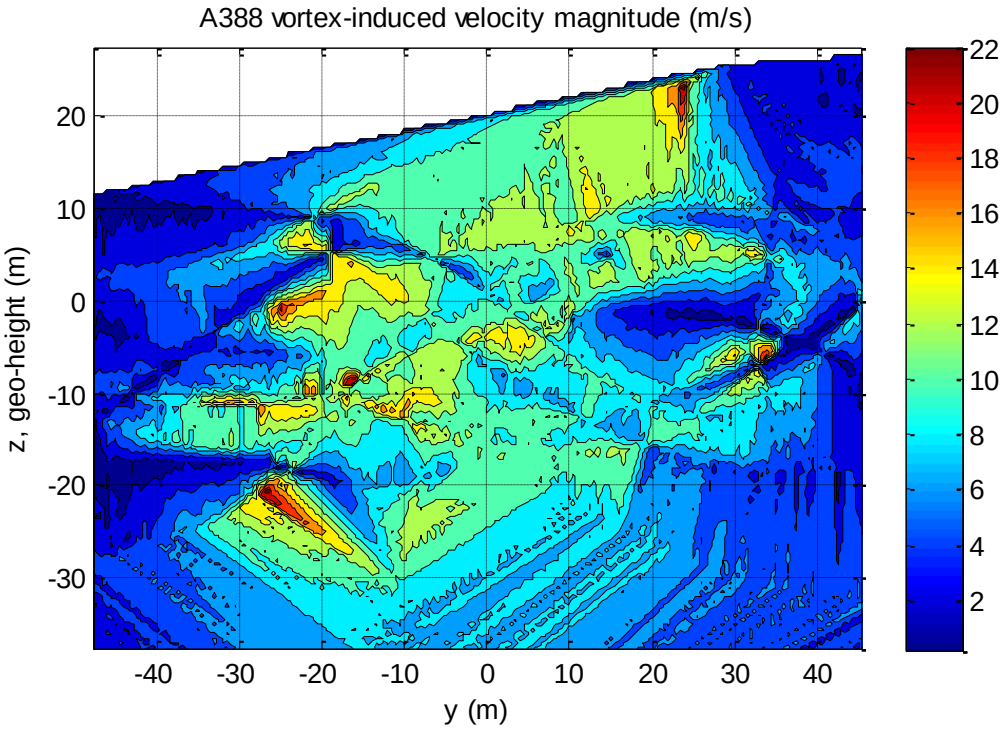

Figure 6 Re-constructed vortex crossplane velocity perturbation field, of a concatenated number of vortex core crossings (red patches); generally mean port-starboard vortex spacings are seen to have been ≈46 m, with apparent long-wave induced variations in vortex spacing.

The lateral transport of the vortex pair (Fig. 7) contained differences to the wind-drift transport. Possibly, the differences evinced effects of background atmospheric shear absorption upon vortex transport. The vortex crossplane background shear was represented by the flight data approximation of quasi-vorticity, which was a sequential spatial forward-differencing of wind component magnitudes, and had the underlying assumption that temporal variations were discountably lower than spatial velocity gradients at the CT-133 flight speed of 0.6 Mach Number, $\omega_{YZi} = \Delta_i w_Z/\Delta_i y - \Delta_i w_Y/\Delta_i z$. It is nevertheless an unsteady quantity. Thus derived, the quasi-vorticity sounding is shown in Fig. 7 also. As expected, it was low, $< 1\ s^{-1}$, at generator height, increasing below the generator. Within the trailing vortex flowfield, patches of quasi-vorticity of 10-100 s^{-1} were derived.

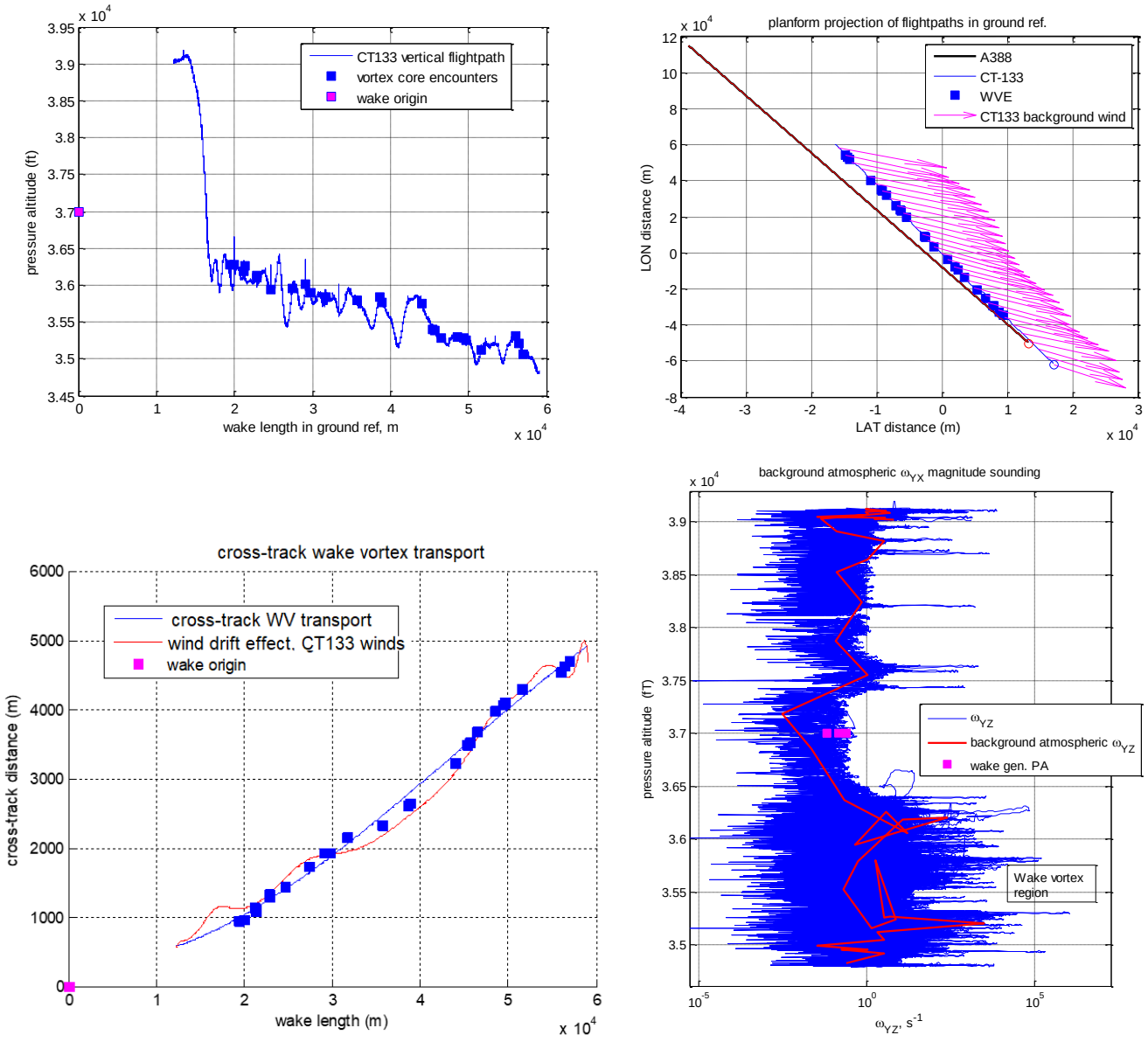

Figure 7 Trailing vortex transport: (*top row*) vertical (*left*) and lateral (*right*); (*bottom row*) lateral transport, (*left*) separating wind drift and vortex drift, and (*right*), sounding of quasi-vorticity, indicating background vorticity increased with displacement below the A388 height, as a potential source of trailing vortex interaction.

B. A359 case, flight data

1. Background stratification and turbulence

The A359 wake survey was conducted north of Ottawa. The generating aircraft was outbound from northeastern North America to Asia, on a Polar route, tracking northwest. Atmospheric conditions consisted of light stratification and light turbulence, at generator height 10.15 km, as shown in Fig. 8.

2. Pressure, temperature and winds

The soundings of measured P, T and winds for the A359 case are presented in Fig. 9, together with the perturbations upon these quantities, induced by the trailing vortex pair. Down-track, the easterly component increased in magnitude, whilst in the sounding manoeuvre (plot domain, 3-3.5$_{10^5}$ pts), both the northerly and easterly components reduced with

increasing altitude. Typical vortex-induced perturbation velocities were of the order of 20 m/s. The wake vortices were both warmer and cooler than the background, as much as +2/-3 K. In the wake vortex cores, pressure expansions of 0.2-0.5 kPa were measured.

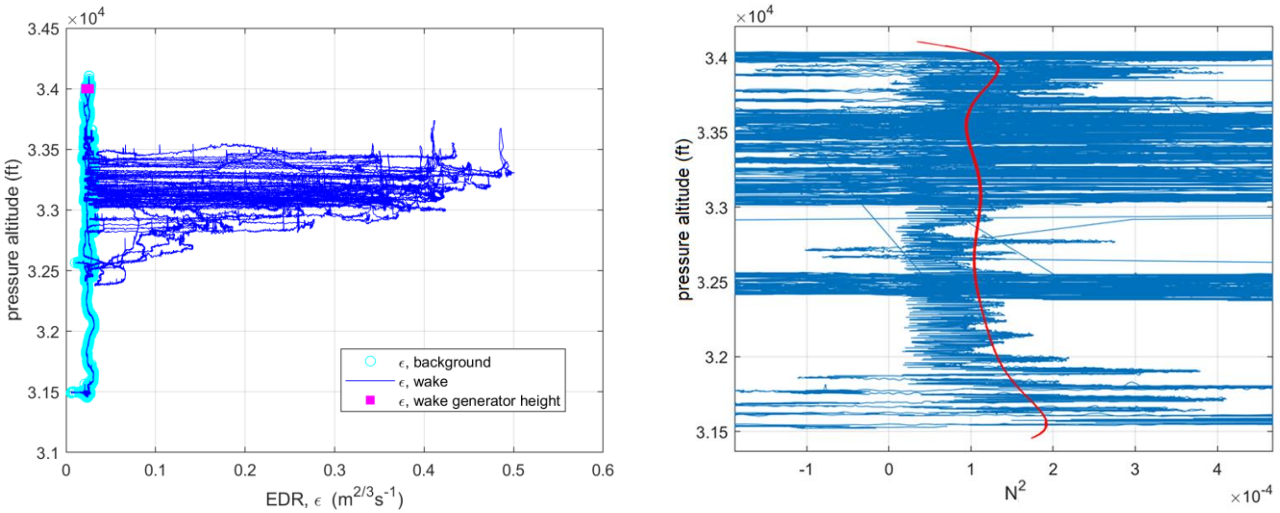

Figure 8 Soundings of atmospheric turbulence (EDR, *left*) and stratification (*right*), A359 flight data, 14th January 2019.

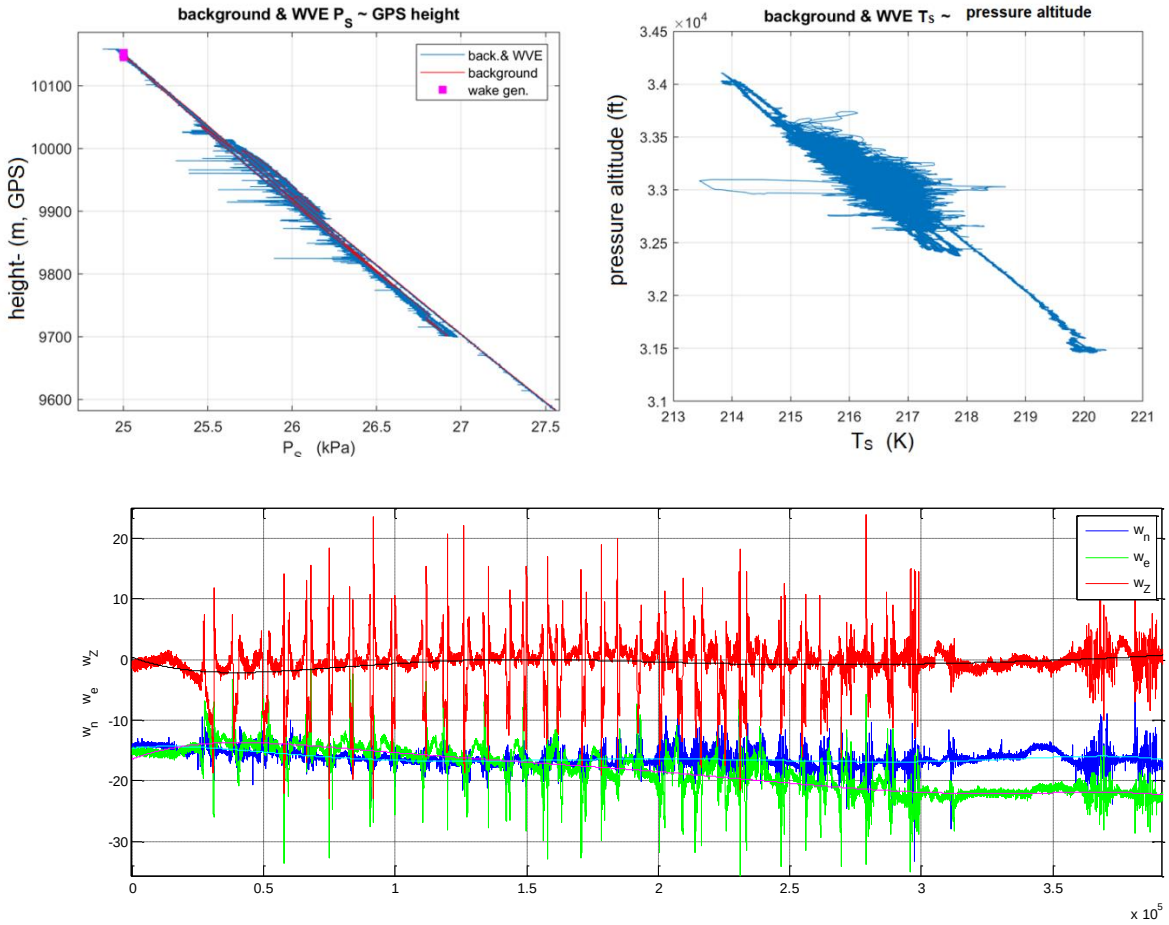

Figure 9 Soundings of atmospheric pressure (*top left*), temperature (*top right*) and timetraces of wind components (*bottom*), A359 flight data, 14th January 2019.

3. Flight data of vortex generation and transport

Principally lateral traverses of the A359 vortex pair were flown, Fig. 10, together with a vertical sounding towards the end of the survey. The behaviour of vortex spacing with age and varying background ε is depicted in Fig. 11, including photographs of vortex state. b_V was measured two ways: optically using a perspective analysis of the splay angle between port and starboard vortices, in the video record of condensate trails, and directly, for the lateral traverses of the CT133 across the vortex pair. ε varied between 0.024 and 0.05 $m^{2/3}/s$, in small-scale turbulence and larger scale shear, respectively, with a mean value of approximately 0.03 $m^{2/3}/s$.

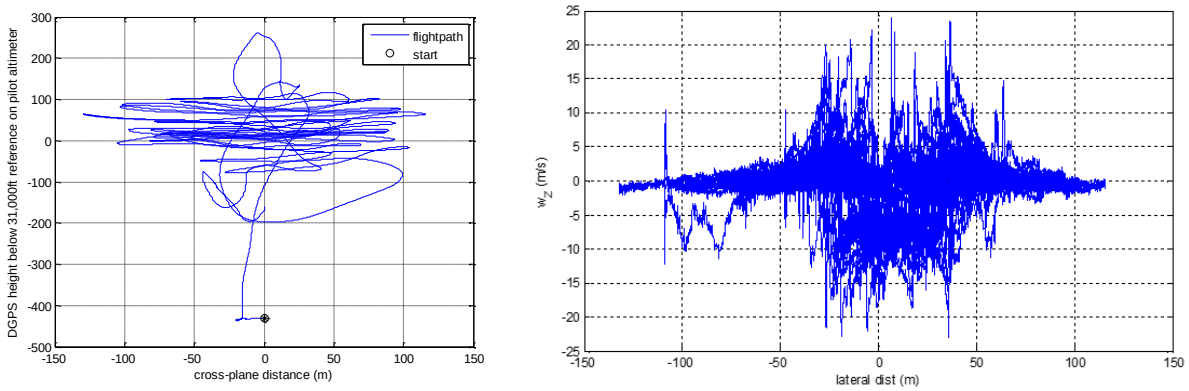

Figure 10 Vortex axis referenced, crossplane flightpath ensemble (*left*), ensemble of vortex core traverse vertical winds (*right*), showing peak induced velocity magnitudes of ±20 m/s and meandering left/right for 40-45 m vortex separation (port vortex at mean lateral distance -19 m, starboard, +24 m.

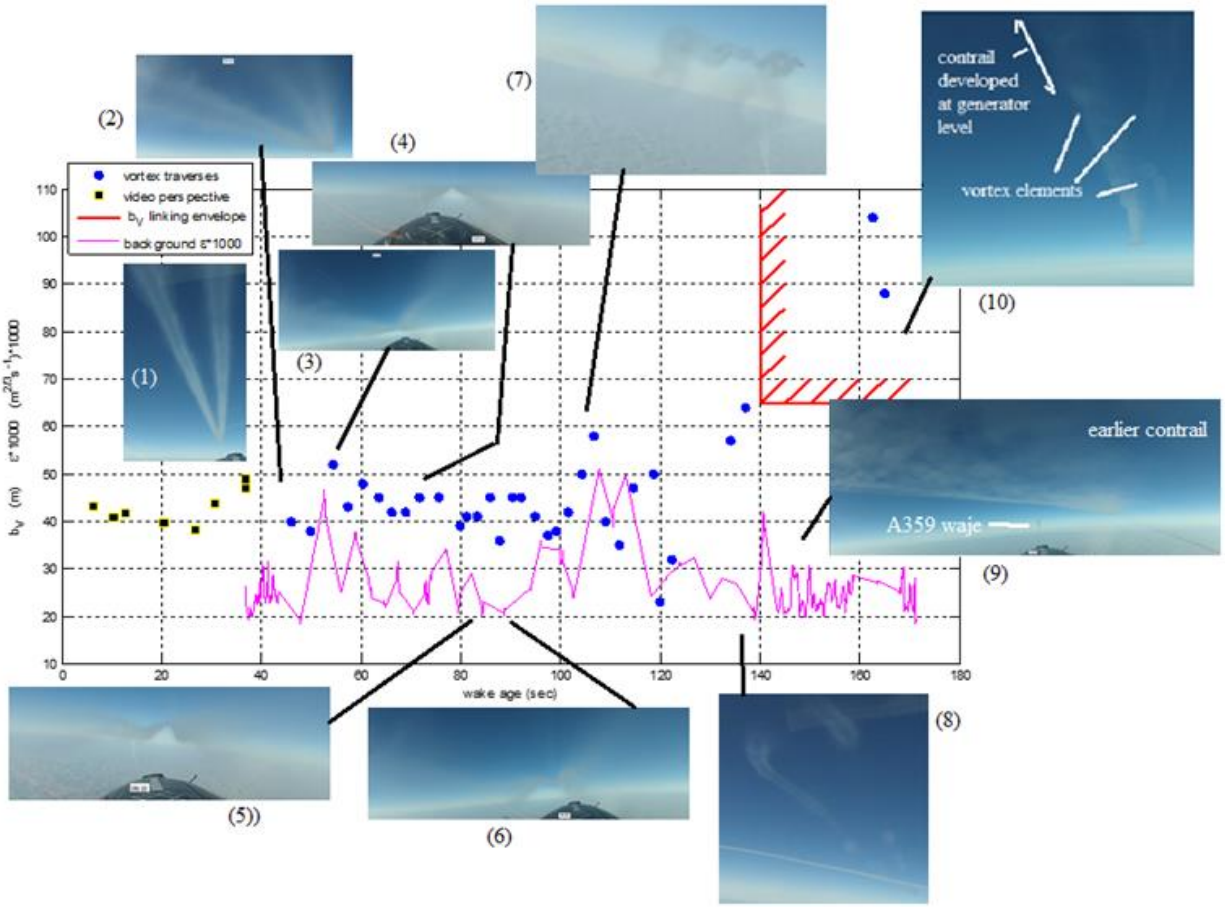

Figure 11 b_V plot against wake age, where b_V derived from video records of optical perspective before WV interception, and by lateral traverses thereafter; subplot of EDR, ε, at WV core traverse height, and an approximate initial WV linking boundary at 140 sec wake age.

The vortex descent path is depicted in Figure 12, together with the lateral drift of the vortex pair, which is the combination of background atmospheric wind drift and atmospheric shear, or other interaction generally.

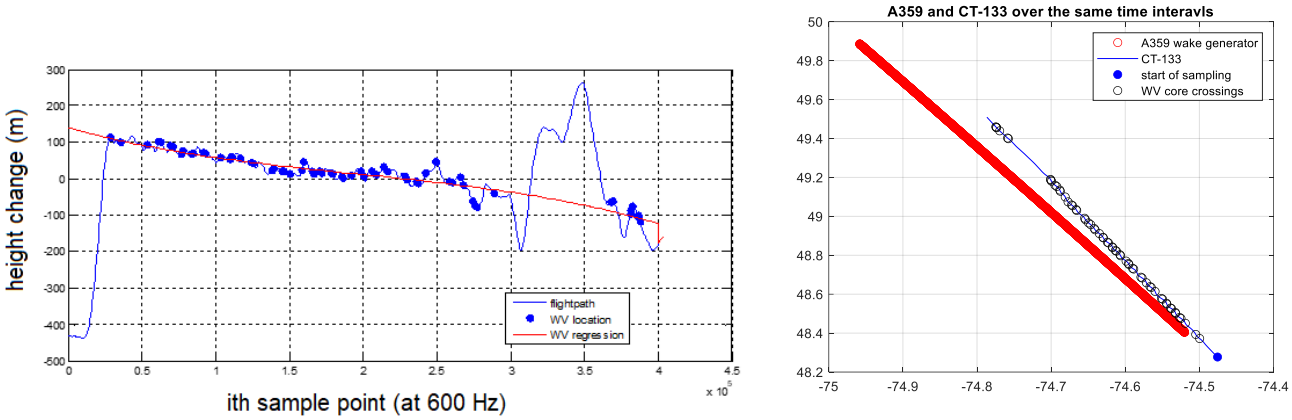

Figure 12 A359 trailing vortex descent path (*left*); planform view of A359 and CT-133 flightpaths (*right*), depicting the combined effects of drift and any atmospheric interactions.

C. DC-8 case, flight data

1. Background stratification and turbulence

The DC-8/CT-133 flight data was gathered during a contrail and emissions research flight, 8th May 2014, on the NASA ACCESS II project [15]. The flight occurred over the Sierra Nevada range of mountains in California. Compared to the other flight cases, the measurement of the generated contrail and wake were initiated closer to the DC-8 wake generator, approximately 2 km behind.

As encountered by the CT-133, ε is presented in Fig. 13, together with a magnified plot of stratification. ε varied between approximately 0.03 and 0.07 $m^{2/3}/s$. The atmosphere was lightly stratified, 0.0003 N^2_{BV}, and displayed an harmonic small-scale variation with altitude, of the same magnitude.

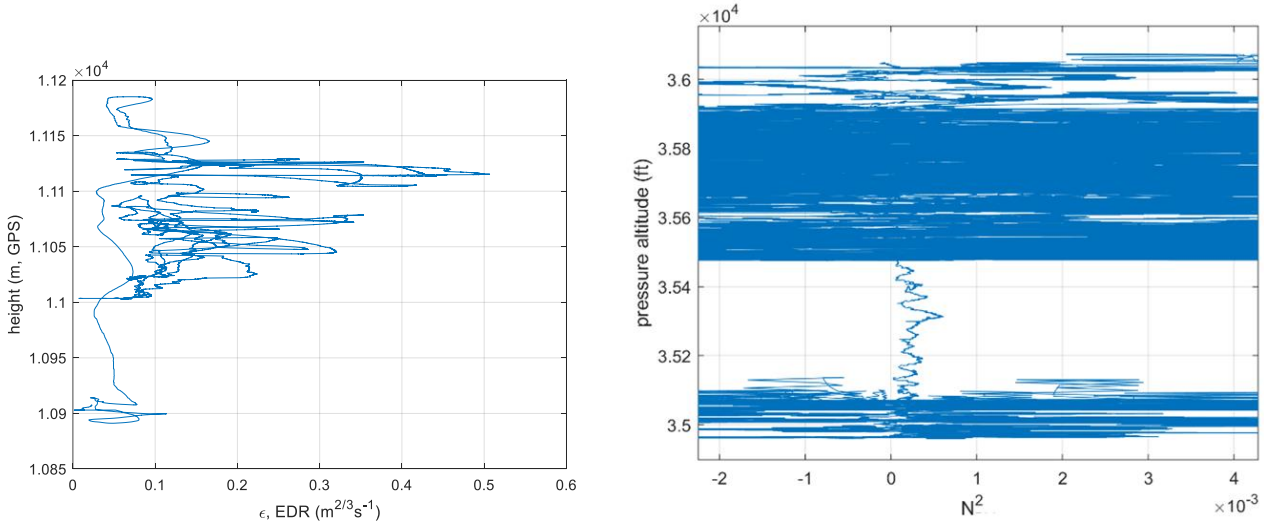

Figure 13 DC-8 flight case, atmospheric turbulence and stratification, as encountered by the NRC CT-133.

2. P, T and winds

Soundings of P, T and northerly/easterly wind components are shown in Fig. 14. It is seen that the trailing vortices were generated in the upper troposphere at 11,147±10 m height. The background temperature lapse rate was slightly non-linear, tropopause onset was possibly 11,230 m. Vortex core-induced pressure expansions were 0.4 to 0.8 kPa, whilst the cores were up-to 4 K warmer than background, generally, with some cool segments, 1 K cooler than background. At 50 m/s, background wind magnitude was high, with a direction essentially parallel to the Sierra Nevada range. The mean values of northerly and easterly wind components had approximately zero lapse rate for the upper 150 m of the sounding. In the lower half of the sounding, magnitude was also similar, but the wind direction backed to the west, with reducing height. Vortex induced wind magnitude variations were as much as ±25 m/s.

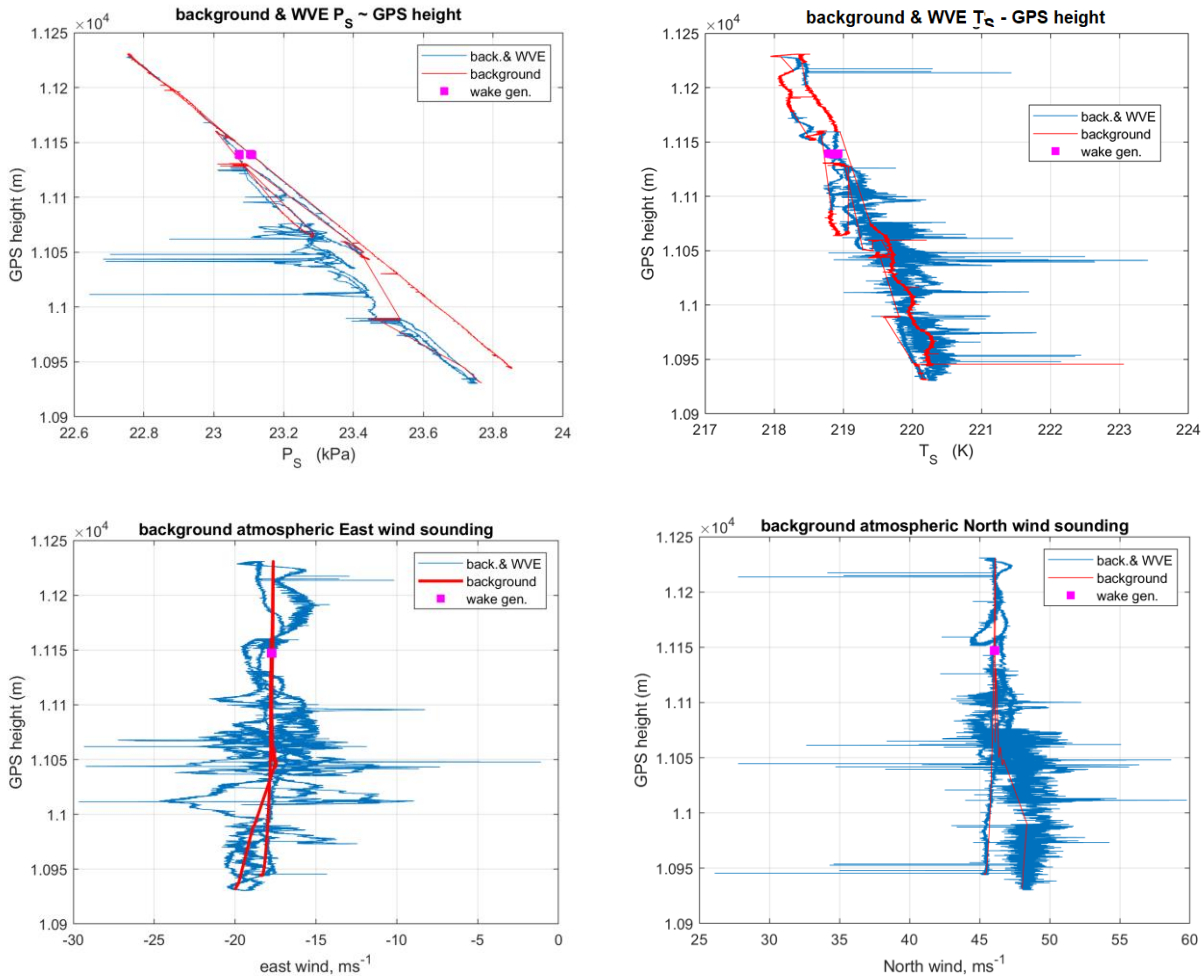

Figure 14 DC-8 flight case, soundings of atmospheric pressure, temperature (*upper plots*) and horizontal winds (*lower*); wake generator height was 11,147±10 m.

3. Trailing vortex generation and transport

Trailing vortex generation is pictorially shown in Fig. 15. For the generator wingspan of 45.2 m, b_V at the average sampled vortex age of 39 sec was 26.75±0.25 m (0.592*b*). At generation, trailing vortex circulation was 372 m^2/s, for this spacing.

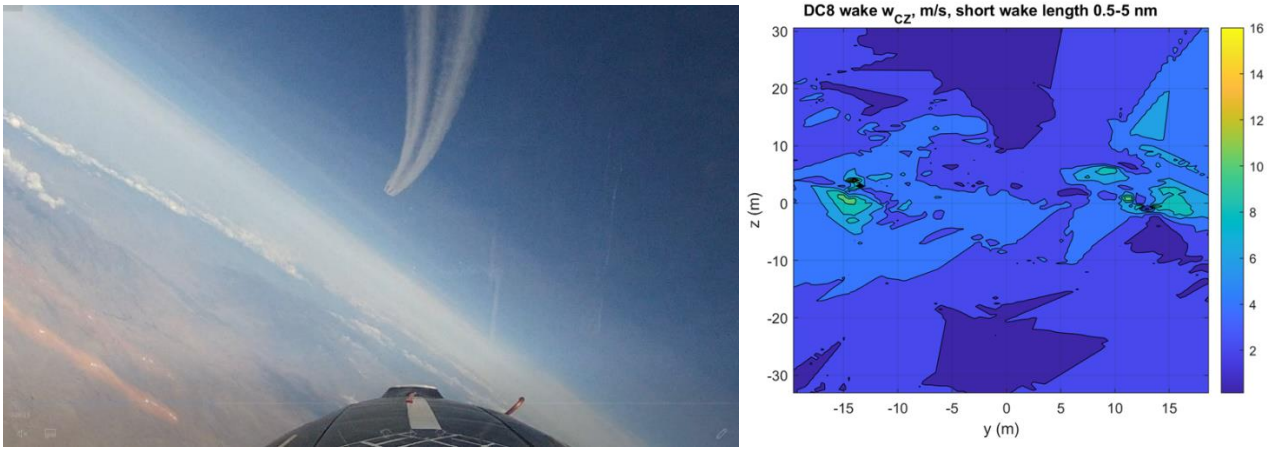

Figure 15 DC-8 flight case, panoramic image of trailing vortices near generation (*left*); contoured and summated plot of vortex velocity magnitudes, from a number of core traverses (*right*).

The trailing vortex descent path, as described by the set of vortex core traverse points, is shown in Fig. 16. A linear regressive fit in Fig. 16, is seen to highlight deviations from a constant vortex descent rate, including the initial entrainment of the shed vorticity sheet (0-4 km). The vortex core traverses have been analysed as gust rise and fall events, Fig. 17. Large amplitude vortex-induced velocities occurred. The rise/fall plot identified two vortex modes, 17 m/s at the small spatial scale of ≈0.17 m, and double that amplitude, 32 m/s at a spatial scale of 1.2m. An example of the larger spatial scale is also shown in Fig. 17, for which the core structure appeared to have been asymmetric, circumferential vortices of the smaller scale size, with a vented core interior between them. The asymmetry suggested an unsteady, transformational vortex state around the core circumference, between core entry and core exit.

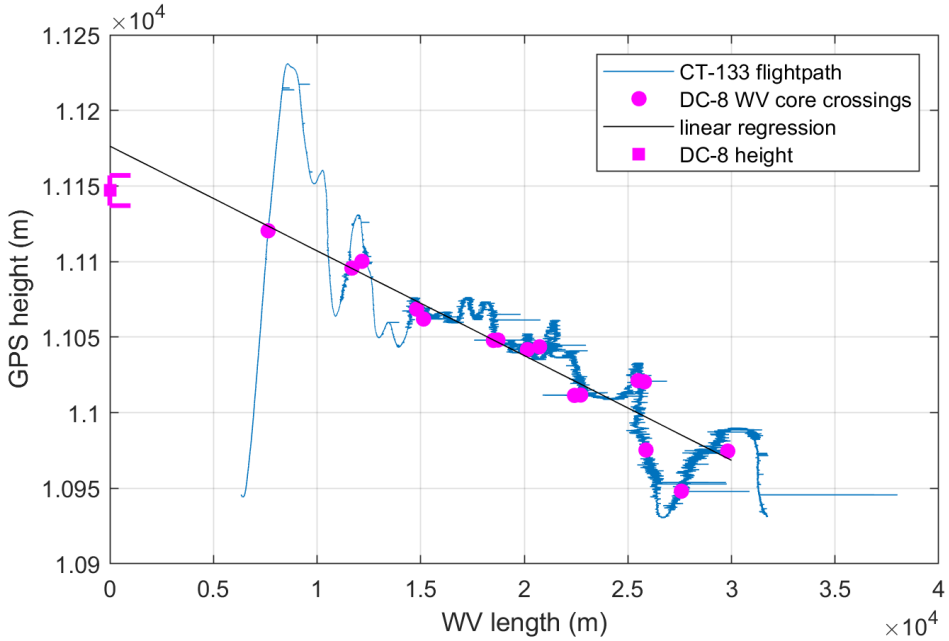

Figure 16 Descent of the DC-8 trailing vortices, with linear regressive fit to the vortex core traverse positions.

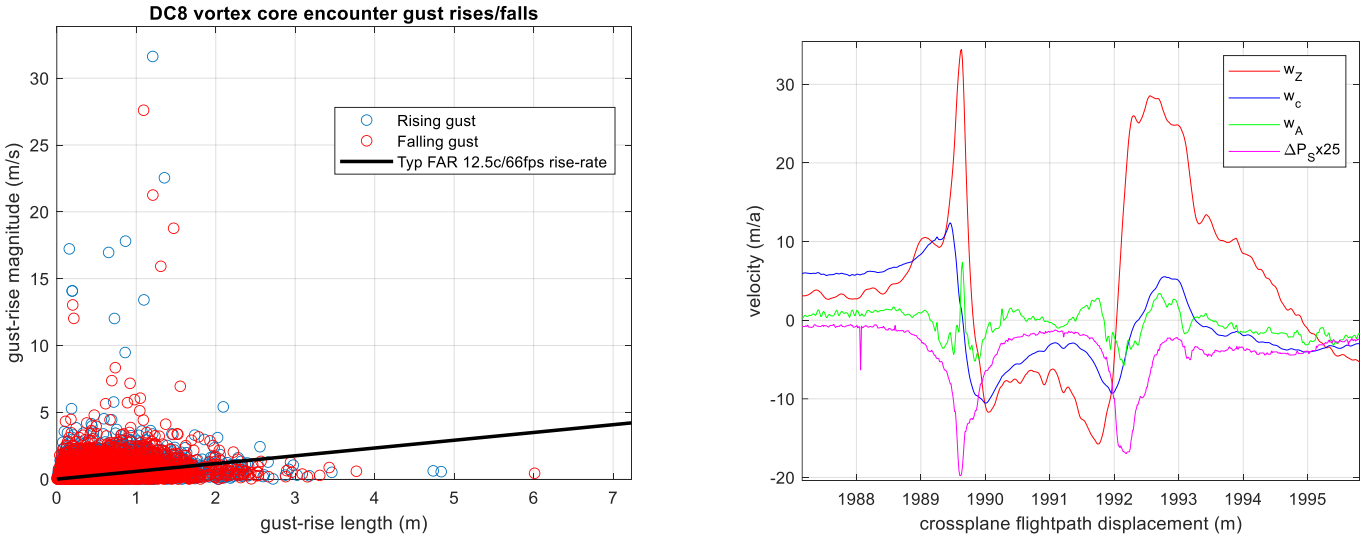

Figure 17 CT-133 traverses of the DC-8 trailing vortices, expressed as gust rise and fall magnitudes (*left*), showing bimodal peaks of 17 m/s at ride length 0.16 m and 32 m/s at 1.2m; a large-amplitude rise/fall pair, equating to a traverse across a core in a vented state, with core radius ≈1.5 m.

V. P2P and P2P^a wake vortex predictions

A. A388 case – predictions with ground-based P2P model

The comparison of the P2P predictions with the CT-133 wake vortex measurements of the A388 case is shown in Fig. 18. The vertical profiles of the meteorological input data, in the height range where the wake vortices evolve, stem from all the CT-133 measurements in the relevant height range, irrespective from the locations where the measurements have actually been taken. As this also includes measurements at similar altitudes but quite remote locations, the profiles partly exhibit substantial jumps which are most pronounced for energy dissipation rate, ε. As P2P employs running averages for the environmental data controlling wake vortex decay [2] (turbulence and thermal stratification), the scatter of this data is tolerable for the P2P prediction quality. The scatter of the wind data, however, would introduce layers with apparent quite pronounced wind shear. Therefore, the wind shear parameterization of P2P [5] has been deactivated for this assessment. Vortex age is computed from the measured vortex length by dividing it by the true airspeed of the A388 of 252 m/s. So, headwind transport of the wake vortices has not to be considered explicitly.

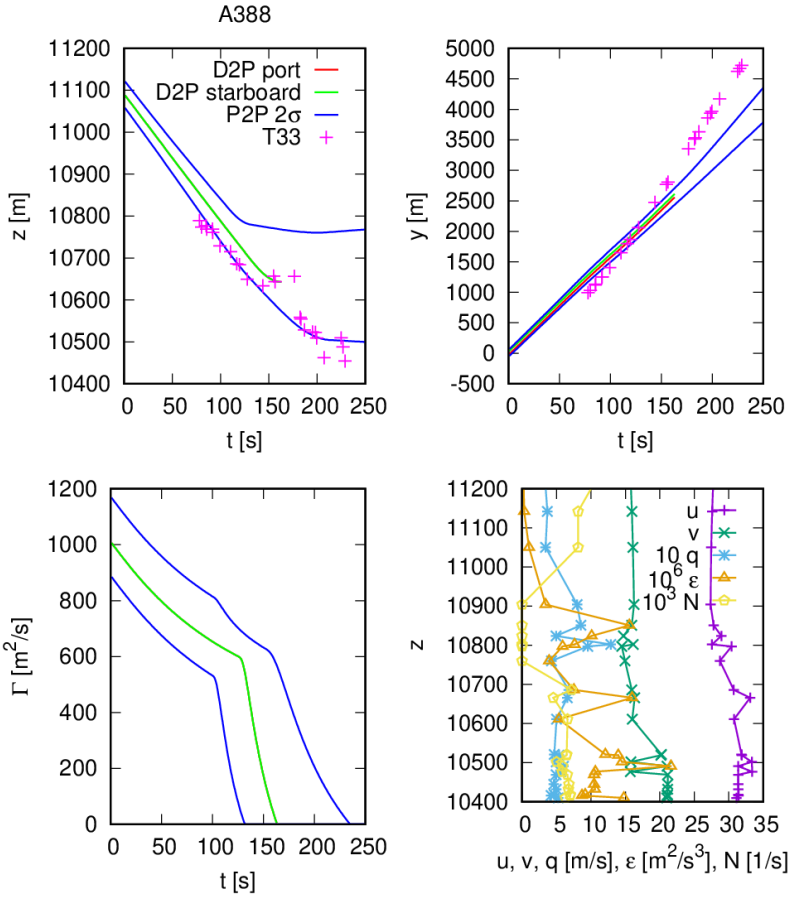

Figure 18 Trailing vortex evolution of A388 aircraft as predicted with P2P model (lines) and measured by the NRC CT-133 (magenta symbols) with vertical profiles of environmental parameters (bottom right). Predictions initialized with measured initial vortex separation of 52.7 m.

In Fig. 18 the mean (deterministic) vortex behavior is denoted by red and green lines for the port and starboard vortices, respectively, while the probabilistic envelopes are blue for the 2-sigma allowances. In the upper left plot for vortex descent, the CT-133 measurements are distributed around the lower probabilistic envelope. The estimated initial circulation (1,011 m²/s) and initial vortex spacing (52.7 m) yield the notably small characteristic vortex time scale t_0 = 17.3 s and also a notably high initial descent speed of w_0 = 3.1 m/s. As the descent speed is well met until a vortex age of about 125 s, the estimated initial values for the circulation and vortex separation appear reliable.

One may argue that the estimated flight altitude of the A388 may be a little too high. Reducing the vortex generation altitude by only 50 m yields a perfect agreement of the measured and predicted deterministic vortex descent (not shown). Note that the measured vortex descent distance is remarkably high covering 637 m. Even if the possibly lower flight altitude of the A388 is considered, the vortex descent distance is still on the order of 2000 ft and thus twice the reduced vertical separation minimum (RVSM) of 1000 ft.

The global height-keeping performance by ICAO[9] specifies height-keeping errors beyond 90 m (300 ft) in magnitude to less than 0.002 probability. Assuming a Gaussian distribution, the 0.002 probability corresponds to 2.9 standard deviations, and thus one standard deviation is estimated to 31 m. So, the 50 m offset is well within that uncertainty, even when the altitude uncertainties of the CT-133 are neglected. Note that the P2P model has been trained employing measurement data collected in ground proximity, where most parameters and, in particular, flight altitude feature substantially smaller uncertainties compared to experiments conducted in cruise conditions.

The lateral vortex drift prediction (Fig. 18 top, right) appears to be close to the measurements. The lateral drift increases in both measurement and prediction when the vortices descend into regions with increasing crosswind at 10,600 m altitude at a vortex age of about 150 s. However, the crosswind transport is somewhat underestimated and the probabilistic envelopes are far too narrow. Again, it should be stated that the model uncertainties are tailored to measurement data collected in ground proximity, where crosswind estimates are more accurate and the resulting predicted probabilistic envelopes are substantially narrower.

Fig. 18 bottom left illustrates the prediction of vortex circulation for which no measurement data is available. The seemingly early end of the prediction of the deterministic vortex lifetime of 163 s appears reasonable as it corresponds to 9.4 vortex time scales, t_0, given the low value of 17.3 s. Potentially, after this vortex rings are forming that can be measured until a vortex age of 226 s which is slightly shorter than the maximum predicted 2-σ envelope for circulation reaching until 234 s.

Fig. 19 illustrates vortex predictions assuming elliptical circulation distribution leading to an initial circulation of $\Gamma_0 = 848$ m²/s and an initial vortex spacing of $b_{V0} = 62.8$ m yielding a vortex time scale of $t_0 = 29.2$ s and an initial descent speed of $w_0 = 2.1$ m/s. Now, even the deterministic vortex lifetime lasts 254 s longer than the vortex observations. However, due to the much smaller initial descent speed magnitude, the observed vortex descent speed and descent distance are clearly underestimated.

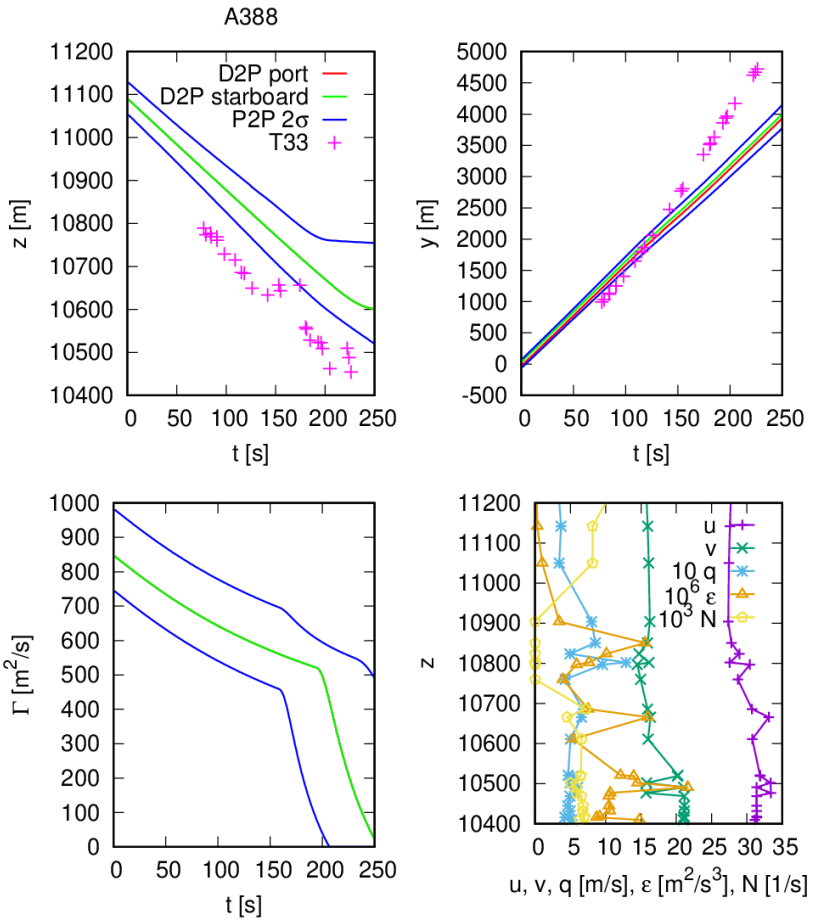

Figure 19 Trailing vortex evolution of A388 aircraft as predicted with P2P model (lines) and measured by CT-133 (magenta symbols) with vertical profiles of environmental parameters (bottom right). Predictions initialized with initial vortex separation of 62.8 m for elliptical circulation distribution.

B. A388 case – predictions with airborne P2P^a model

The input parameters employed for the wake vortex predictions with the airborne P2P^a model are listed in Table 1. For all parameters an estimate of the average value and a respective standard deviation is prescribed. Additionally, for wind, turbulence, and thermal stratification the respective vertical gradients are included. For the latter meteorological parameters, the average values on flight altitude and their standard deviations as well as the vertical gradients are derived from linear fits to the measurement data gathered by the CT-133.

Fig. 20 shows the comparison of the P2P^a predictions with the CT-133 wake vortex measurements of the A388 case. For the uncertainty allowances a 95% probability has been selected. Fig. 20 bottom right depicts the meteorological parameters as used by the four internal P2P^a prediction runs. For every meteorological parameter at least one vertical profile for minimum values and one for maximum values are generated to support the prediction of the envelopes of the vortex parameters with the selected 95% probability.

Table 1 Input parameters for P2P^a for A388 case

parameter	value	standard deviation	gradient
mass	495010 kg	1000 kg	-
vortex separation	52.7 m	4.7 m	-
true airspeed	252 m/s	2 m/s	-
true heading	338.4°	1°	-
height	11091 m	31 m	-
air density	0.362 kg/m³	0.001 kg/m³	-
wind speed	29.6 m/s	1.1 m/s	-0.0129 1/s
wind direction	124.2°	2.6°	$-9.26\cdot10^{-4}$ °/m
energy dissipation rate	$2.38\cdot10^{-6}$ m²/s³	$4.22\cdot10^{-6}$ m²/s³	$1.83\cdot10^{-8}$ m/s³
potential temperature	324.7 K	0.27 K	$1.90\cdot10^{-3}$ K/m

For illustration purposes, the plots of vortex position and strength also comprise the results of the four internal P2P^a runs denoted z_{min}, z_{max}, t_{min}, and t_{max}. For vortex circulation, Γ, shown in Fig. 20 bottom left, these runs define directly the blue probabilistic envelopes, while for vortex position the curves produced by the internal runs are expanded by superposition of the variances of various relevant input parameters.

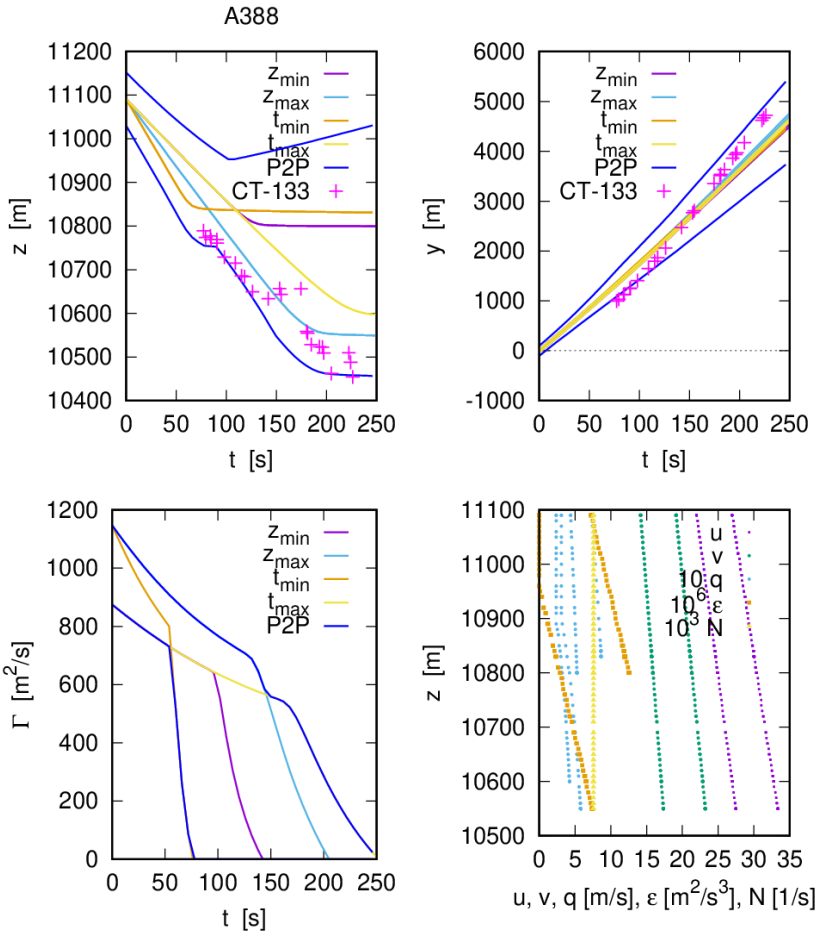

Figure 20 Trailing vortex evolution of A388 aircraft as predicted with airborne P2P^a model (lines) and measured by CT-133 (magenta symbols) with vertical profiles of environmental parameters (bottom right). Predictions initialized with measured initial vortex separation of 52.7 m.

A comparison of Fig. 18 and Fig. 20 clearly elucidates that the uncertainty allowances of the airborne version P2P^a are substantially larger than those of the ground-based P2P. As a consequence, all the measurements for vortex descent reside within the probabilistic envelope of P2P^a while for lateral transport this is mostly the case with the exception of a period ranging from 77 s to 91 s.

Fig. 21 illustrates the P2P^a predictions assuming elliptical circulation distribution with an initial vortex spacing of b_{V0} = 62.8 m (wing span b = 79.75 m) and without any standard deviation. First of all, it is noticeable that with zero standard deviation of the initial vortex separation the runs for z_{min}, t_{min} and z_{max}, t_{max} almost fall on top of each other, respectively, while the lifetime range is increased compared to the case employing the smaller initial b_{V0} of the more compact measured vortex pair. Again, like in Figure 19 for P2P, the much smaller descent speed does not meet the observed vortex descent speed and yields a substantially smaller descent distance. Combining the elliptical b_{V0} with a standard deviation that would enclose the observed descent distances, would yield excessively large probabilistic envelopes.

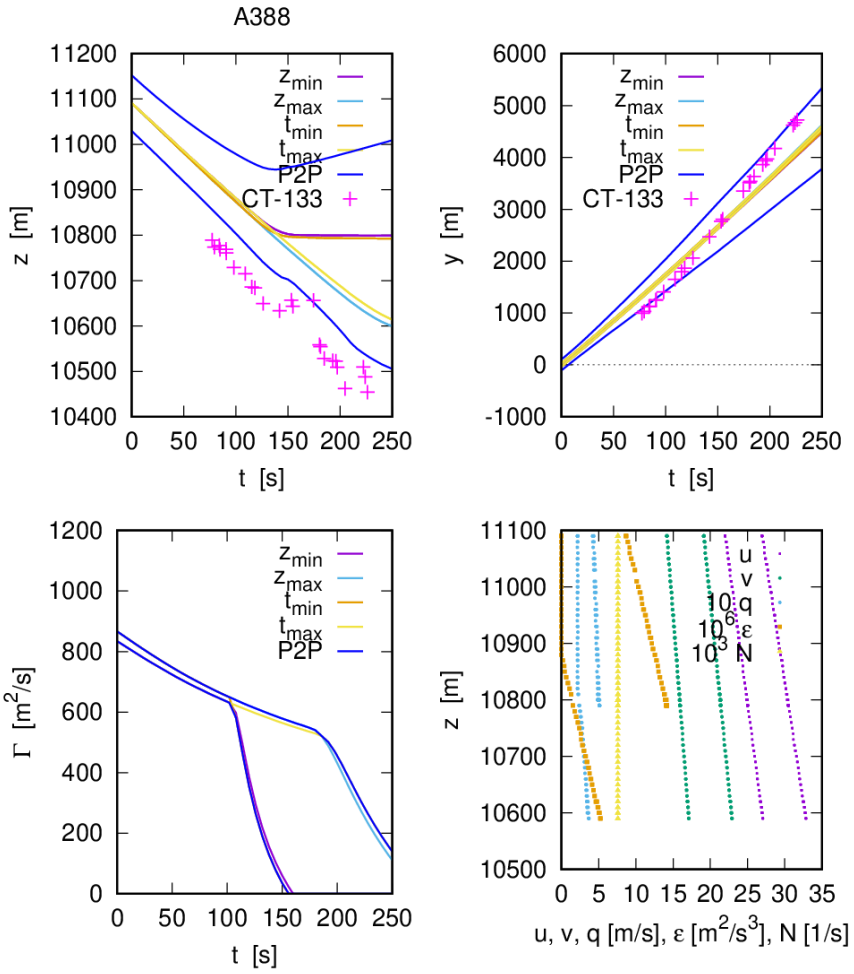

Figure 21 Trailing vortex evolution of A388 aircraft as predicted with airborne P2P^a model (lines) and measured by CT-133 (magenta symbols) with vertical profiles of environmental parameters (bottom right). Predictions initialized with initial vortex separation of b_{V0} = 62.6 m for elliptical circulation distribution and zero standard deviation.

C. A359 case – predictions with ground-based P2P model

Fig. 22 depicts the P2P predictions of the evolution of the wake vortices generated by the A359 aircraft together with the underlying CT-133 measurements. The predictions are initialized with a vortex separation of b_{V0} = 43.4 m which is an average of measurements taken between vortex ages from 10 s to 100 s and an initial circulation of

585 m²/s estimated from flight data. The comparison of predictions with measurements yields a quite similar picture as for the A388 case such that many comments made in sections V.A and V.B also hold here.

Again, the measured vortex descent is distributed around the lower 95% envelope. With a decrease of the A359 flight altitude of only 50 m, the measurements would be equally distributed around the deterministic prediction (green line) except the late measurements after 122 s (not shown). The late altitude measurements feature substantial height variations indicating that the sinusoidal deformation of Crow instability[10] or even the subsequent stage of the formation of vortex rings has set in. Again, as for the A388, using the initial separation of b_{V0} = 50.9 m, resulting from the assumption of an elliptical circulation distribution, yields a clear underestimation of the descent speed (not shown).

The uncertainty allowances for lateral vortex position appear far too small. Also, the lateral transport resulting directly from the crosswind profiles features opposite trends of measurement and prediction; at a vortex age around 70 s the lateral transport speed is increased in the measurements while it is reduced in the predictions. So, although the mean lateral transport speed is well met, there is substantial uncertainty in the crosswind field, which is not considered adequately by the P2P model calibrated with measurement data collected in ground proximity at airports.

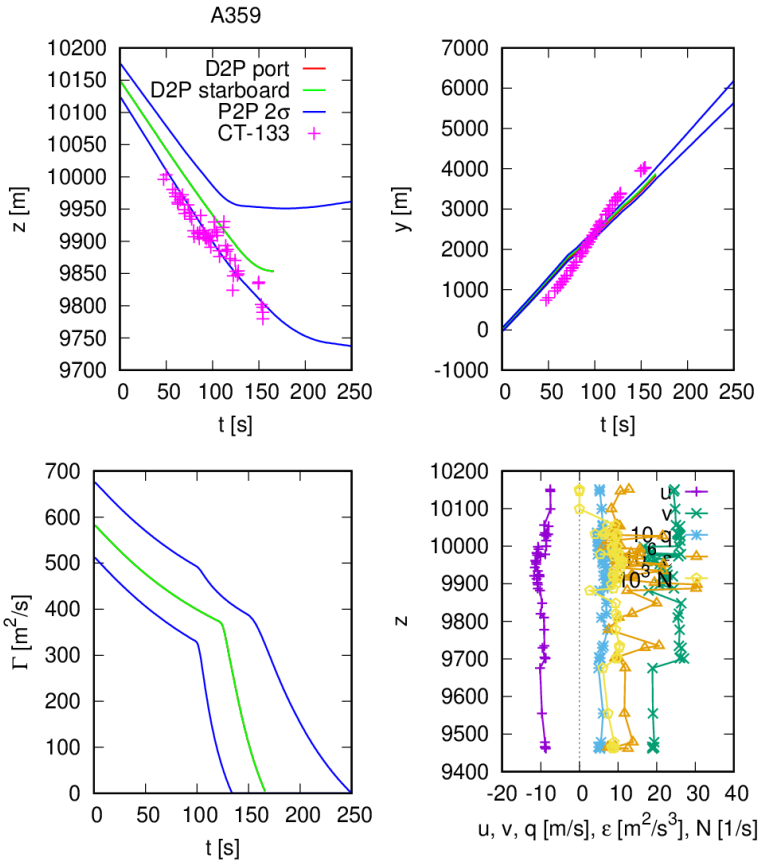

Figure 22 Trailing vortex evolution of A359 aircraft as predicted with P2P model (lines) and measured by CT-133 (magenta symbols) with vertical profiles of environmental parameters (bottom right). Predictions initialized with measured initial vortex separation of 43.4 m.

D. A359 case – predictions with airborne P2P^a model

Fig. 23 shows the comparison of the P2P^a predictions with the CT-133 wake vortex measurements of the A359 case. The input parameters employed for the wake vortex predictions with the airborne P2P^a model are listed in Table 2. Using the standard deviations of the input parameters derived from the scatter of the measurement data, almost all measured vortex positions reside within the probabilistic envelopes. The lower probabilistic envelope for vortex descent just encloses the measured descent distances, while the descent speeds seen in the measurements and the predictions correspond very well. With a descent distance of 370 m also the wake vortices generated by the A359

reach the next flight level 1000 ft below, even when uncertainties of the flight altitudes are considered. The envelopes for lateral transport mostly enclose the measurement data thanks to the high standard deviations of wind speed and direction even though the average lateral transport speed is not so well met and the model design does not foresee nonlinear vertical wind gradients.

So, the P2P^a model design appears to be well-suited to deal with the substantial uncertainties of the input parameters as they typically occur during cruise operations. One example of how the model copes with these uncertainties, which appears not so successful in this case though, is the climb of the upper probabilistic envelope for vertical position after 90 s. This climb is caused by the quite high standard deviations of wind speed and direction, as these could also be related to substantial vertical wind shear that might trigger vortex rebound [11,12] which, however, is not the case here.

Table 2 Input parameters for P2P^a for A359 case

parameter	value	standard deviation	gradient
mass	256240 kg	1000 kg	-
vortex separation	43.5 m	0.1 m	-
true airspeed	243.4 m/s	2 m/s	-
true heading	342.4°	1°	-
height	10150 m	31 m	-
air density	0.407 kg/m³	0.0025 kg/m³	-
wind speed	25.5 m/s	2.6 m/s	0.00241 1/s
wind direction	49.4°	5.4°	-0.000926 °/m
energy dissipation rate	$9.58 \cdot 10^{-6}$ m²/s³	$5.77 \cdot 10^{-6}$ m²/s³	$-2.28 \cdot 10^{-8}$ m/s³
potential temperature	319.2 K	0.181 K	0.0037 K/m

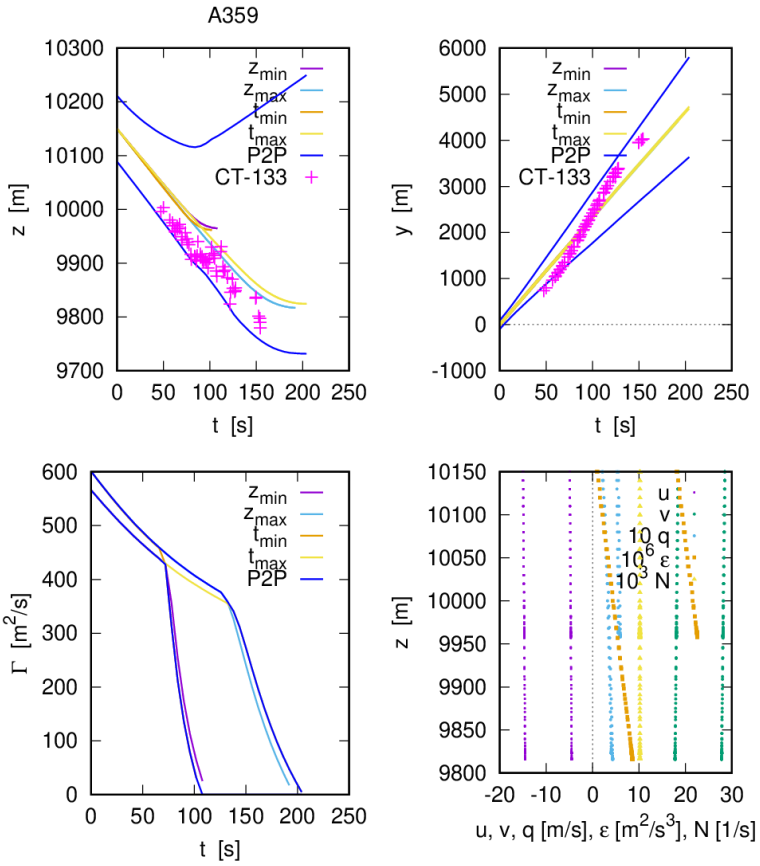

Figure 23 Trailing vortex evolution of A359 aircraft as predicted with airborne P2P^a model (lines) and measured by CT-133 (magenta symbols) with vertical profiles of environmental parameters (bottom right). Predictions initialized with values listed in Table 2.

E. DC-8 case – predictions with ground-based P2P model

Fig. 24 depicts the P2P predictions of the DC-8 case for which only the measured vortex descent data is available. The predictions are initialized with the measured initial vortex separation of b_{V0} = 26.8 m which is even 24.5% smaller than the theoretical value of b_{V0} = 35.5 m for elliptical circulation distribution. Although the environmental data exhibits noticeable spikes for the energy dissipation rate (bottom right), the predicted vortex descent rate and lifetime compare well with the CT-133 measurements. Obviously, the running average used for stratification and turbulence parameters[3], which allows a weighting of the impact of the environmental conditions according to the respective residence time of the vortices at a particular vertical position, limits the effects of these peaks. Again, the spread of the vertical vortex positions increases for older vortex ages (after about 85 s), indicating that the vortex lines are not straight anymore and may establish sinusoidal instabilities.

The flight altitude of the DC-8 is probably underestimated, in contrast to the two Airbus cases presented above, such that the first five measured altitudes reside above the 95% envelope. The use of the theoretical initial vortex separation of b_{V0} = 35.5 m yields a substantially smaller initial vortex descent speed such that all the measured descent distances are situated within the probabilistic envelopes (not shown).

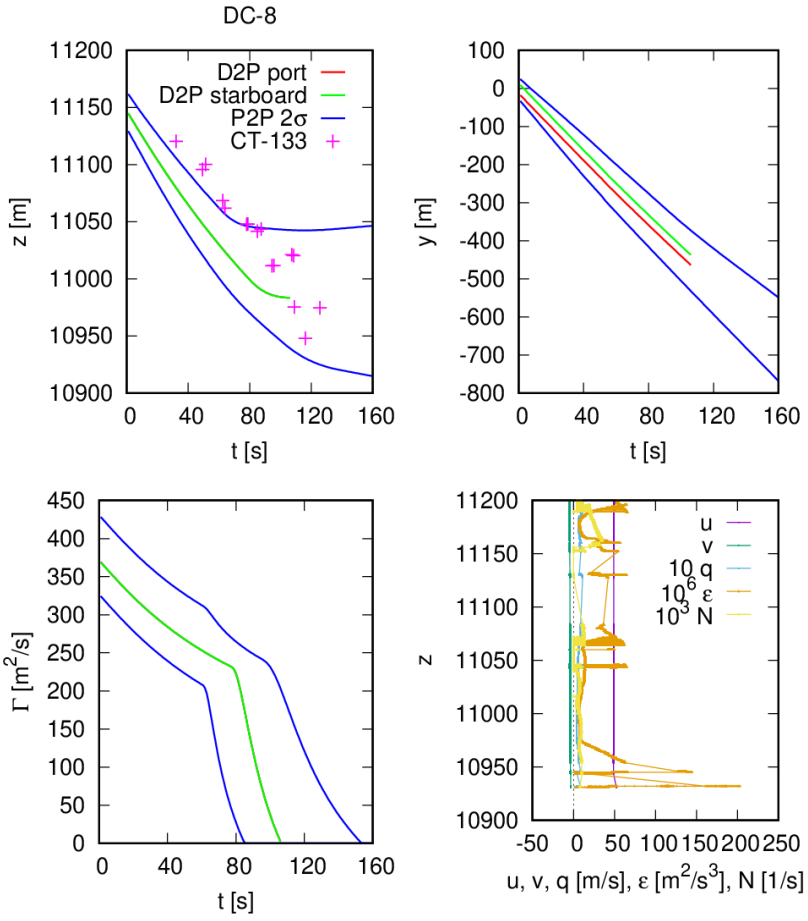

Figure 24 Trailing vortex evolution of DC-8 aircraft as predicted with P2P model (lines) and measured by the NRC CT-133 (magenta symbols) with vertical profiles of environmental parameters (bottom right). Predictions initialized with measured initial vortex separation of 26.8 m.

F. DC-8 case – predictions with airborne P2P^a model

Fig. 25 compares P2P^a predictions with the measurements employing the input data listed in Table 3. Using the uncertainty of the flight altitude of 31 m, the measured vortex descent is well within the probabilistic envelopes.

Despite the small characteristic vortex time scales, t_0, between 11 s and 13 s resulting from the small initial b_{V0} of 26.75 m, also wake vortex lifetime is well met, as the internal P2P^a runs for maximum vortex lifetime and descent use the low energy dissipation rates resulting from the substantial scatter ($\sigma_\varepsilon = 1.94 \cdot 10^{-5}$ m²/s³) of the measured ε-profiles. In Fig. 25, P2P^a appears again well suited to predict wake vortex behaviour during cruise by considering the typically large uncertainties of the input parameters during this phase of flight.

Table 3 Input parameters for P2P^a for DC-8 case

parameter	value	standard deviation	gradient
Mass	88290 kg	1000 kg	-
vortex separation	26.75 m	0.25 m	-
true airspeed	237.3 m/s	2 m/s	-
true heading	333.8°	1°	-
Altitude	11147 m	31 m	-
air density	0. 367 kg/m³	0.001 kg/m³	-
wind speed	49.6 m/s	0.22 m/s	0.00269 1/s
wind direction	159.2°	0.35°	0.00455 °/m
energy dissipation rate	$3.25 \cdot 10^{-5}$ m²/s³	$1.94 \cdot 10^{-5}$ m²/s³	$2.79 \cdot 10^{-8}$ m/s³
potential temperature	333.9 K	0.153 K	0.00469 K/m

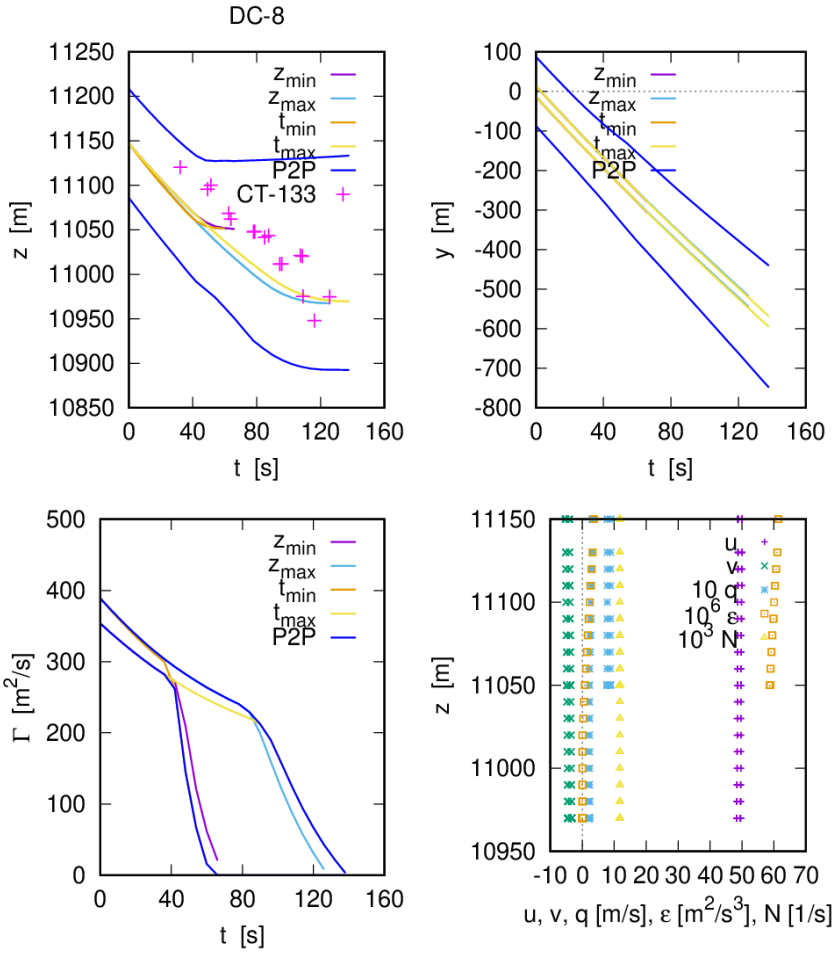

Figure 25 Trailing vortex evolution of DC-8 aircraft as predicted with airborne P2P^a model (lines) and measured by CT-133 (magenta symbols) with vertical profiles of environmental parameters (bottom right). Predictions initialized with values listed in Table 3.

G. Discussion

As we present only a few selected cases, one may argue whether these represent rather typical conditions for cruise or not. Vortex lifetimes and descent distances are mainly controlled by thermal stratification (here Brunt-Väisälä frequency, N) and turbulence energy dissipation rate, ε, which in these cases vary within the limits $0 \leq N \leq 0.012$ s^{-1} and $2 \cdot 10^{-6}$ m²/s³ $\leq \varepsilon \leq 3 \cdot 10^{-5}$ m²/s³, respectively. According to Ref. [8], these ranges of N and ε are well within the range of atmospheric conditions prevailing at cruise altitudes collected from various in situ observations. So, one may conclude that the presented cases are typical of cruise conditions.

The measured initial vortex separations are about 15% smaller than those expected from elliptical circulation distribution for the Airbus planes and 24.5% smaller for the DC-8. The presented P2P and P2P^a predictions elucidate that the b_{V0} values have a very strong effect on wake vortex lifetime and descent distance. The spanwise load factor s, which relates the initial vortex separation, b_{V0}, to the wing span, b, according to $s = b_{V0}/b$, amounts to $\pi/4$ for an elliptical spanwise circulation distribution. Here it is briefly listed how deviations of the load factor from this theoretically ideal value may affect wake vortex predictions. The initial circulation $\Gamma_0 = \frac{mg}{\rho s b V}$ is inversely proportional to s, where m is aircraft mass, g gravitational acceleration, ρ is air density, and V is true airspeed. However, the characteristic wake vortex time scale $t_0 = 2\pi \frac{b_0^2}{\Gamma_0}$, which scales with dimensional vortex lifetimes, is proportional to s^3. So, the descent speed $w_0 = \frac{b_0}{t_0}$ is proportional to s^{-2}. Further, it should be noted that also the effects of the environmental parameters on vortex lifetime depend on s according to $N^* = N t_0$ scaling with s^3 and $\varepsilon^* = \frac{(\varepsilon b_0)^{1/3}}{w_0}$ scaling with $s^{7/3}$. So, with a maximum dependence of these key wake vortex parameters on s^3, the noticed 15% deviation may change results by about 40%. For the DC-8 this impact may even reach almost 60%.

This little exposition illustrates the significant relevance of the knowledge of the initial vortex separation for any consideration related to vortex lifetimes and descent distances during cruise. For an onboard wake vortex prediction system[13], it appears crucial to consider these tighter initial vortex separations either by establishing an aircraft type specific data base or by determining average deviations from elliptical spanwise load factors combined with appropriate uncertainties. For approach and landing it would be worthwhile to also know how b_{V0} changes in high-lift conditions[14].

Finally, the presented P2P^a predictions illustrate that for onboard wake vortex predictions with reasonably small wake vortex warning areas a good knowledge of the wind field is mandatory. Even in the current case where a research aircraft was measuring the wind field, however, in large regions not restricted to where the vortices actually evolved, quite huge wake warning areas appear unavoidable. At the end of the maximum wake vortex lifetime of the A388 case at t = 246 s in Figure 2, the width of the vertical 95% envelope amounts to about 570 m and the lateral envelope to about 1600 m. The corresponding dimensions of the A359 case in Figure at t = 192 s are vertically about 500 m and horizontally about 2000 m. A dedicated reconstruction of the wind field along the aircraft track using wind measurements of the involved aircraft pair, possibly combined with numerical weather prediction data in particular for estimating the respective vertical gradients, may reduce the huge dimensions of the wake vortex warning areas to a size that might be acceptable in terms of the number of wake vortex warnings that would not lead to wake vortex encounters if they were ignored.

VI. Conclusions

Flight data of the trailing vortices of the three aircraft types A388, A359, and DC-8 during cruise flight has been obtained with the NRC CT-133 research aircraft. Trailing vortex lateral spacing and transport were measured and background atmospheric data derived for input into two versions of the Probabilistic 2-Phase wake vortex prediction model – the ground-based P2P model and its airborne version P2P^a. To the authors' knowledge there are almost no publications dealing with fast-time wake vortex model predictions in cruise conditions. The current paper fills this gap by demonstrating and analyzing the prediction skills of two wake vortex model versions under cruise conditions.

The flight data was obtained in low turbulence and light stratification. Wind sounding magnitude and directional lapses indicated non-zero levels of background atmospheric shear. The degrees of thermal stratification and turbulence energy dissipation rates prevailing during the CT-133 measurements were well within the range of atmospheric conditions collected from various in situ observations at cruise altitudes [8]. As these two parameters mainly control wake vortex lifetimes and descent, the presented cases can be considered typical for wake vortex evolution in cruise conditions.

It is noteworthy that the vortex descent distance measured in the A388 case covers more than 2000 ft and thus about twice the reduced vertical separation minimum (RVSM) of 1000 ft. This means that pilots following or crossing the track of an A388 one flight level below should be aware of the risk of an imminent encounter and should use an upwind flight track whenever possible. The A359 case illustrates that also the wake vortices generated by other heavy aircraft types may reach down to the next flight level 1000 ft below.

The predictions of two versions of the P2P wake vortex model were compared to the flight data. While the ground-based P2P model failed to predict appropriate probabilistic envelopes mainly for the lateral transport of the wake vortices, the 95%-envelopes predicted by the airborne version P2P^a embraced successfully most of the CT-133 measurement data. These different model performances are expected and related to the different probabilistic model designs. While the established P2P version uses ground-based measurement data to calibrate its probabilistic envelopes [5], the runtime optimized airborne version P2P^a uses uncertainties of all relevant impact parameters to construct the probabilistic envelopes [7]. Ground based measurements feature substantially higher accuracies as airborne measurements, where the environmental data may be gathered partly in air masses far off those that actually control wake vortex behavior.

Successful predictions of the vortex descent speed and distance by both models require the knowledge of the true initial vortex separation b_{V0}, which was determined by the measurements to be by 15% to almost 25% smaller than the b_{V0} values expected from elliptical circulation distributions. Such large deviations of the spanwise load factor, s, affect wake vortex prediction results significantly, as key wake vortex parameters have a dependence on s of up to the power of three. The presented cases also demonstrate that the successful prediction of vortex descent has to consider the uncertainty of the flight altitude of the vortex generator. The standard deviation of 31 m derived from estimates by ICAO [9] appears appropriate.

As P2P and P2P^a predict well the average vortex descent speeds and vortex lifetimes and as they employ the same dynamical core, one may conclude that the physics of wake vortex behavior is sufficiently well represented by both P2P model versions. The suitability for either ground-based or airborne applications is mainly connected to the different methods for the consideration of the uncertainties of the aircraft and environmental parameters for the prediction of the probabilistic envelopes.

Provided that reasonable estimates of the uncertainties of the input parameters are available, the P2P^a model appears to be well suited for onboard wake vortex prediction [7]. In order to attain good wake vortex predictions with acceptable dimensions of the probabilistic wake vortex envelopes, a model or data base of initial vortex separations should be established and the uncertainties of the crosswind should be minimized. The latter may be achieved by a dedicated reconstruction of the wind field along the aircraft track using wind measurements of the involved aircraft pair, possibly combined with numerical weather prediction data in particular for estimating the respective vertical gradients.

Acknowledgments

The 2006-2021 enroute wake vortex NRC flight research was conducted under the sponsorship of the National Research Council Canada and the Federal Aviation Administration of the United States of America. Part of the development of P2P^a has been performed under contract to Airbus and the support received is gratefully appreciated. The investigations have received funding from the German Aerospace Research Center (DLR) project NICo (Next Generation Intelligent Cockpit).

References

[1] Brown, A.P., "Identification of Trailing Vortex Dynamic States," doi: 10.5772/intechopen.110787, 13th April 2023, from the edited volume "Vortex Simulation and Identification [Working Title]," Dr Chaoqun Liu, published by IntechOpen.

[2] Holzäpfel, F., Gerz, T., "Aircraft Wake Vortices: From Fundamental Research to Operational Application, Research Topics in Aerospace, Atmospheric Physics - Background - Methods - Trends," U. Schumann Editor, Springer, 2012, pp. 219-237, ISBN 978-3-642-30182-7,ISBN 978-3-642-30183-4, https://doi.org/10.1007/978-3-642-30183-4.

[3] Holzäpfel F., 2003: Probabilistic Two-Phase Wake Vortex Decay and Transport Model, Journal of Aircraft, Vol. 40, No. 2, pp. 323-331, https://doi.org/10.2514/2.3096.

[4] Holzäpfel F., Robins R.E., 2004: Probabilistic Two-Phase Aircraft Wake Vortex Model: Application and Assessment, Journal of Aircraft, Vol. 41, No. 5, pp. 1117-1126, https://doi.org/10.2514/1.2280.

[5] Holzäpfel F., 2006: Probabilistic Two-Phase Aircraft Wake-Vortex Model: Further Development and Assessment, Journal of Aircraft, Vol. 43, No. 3, pp. 700-708, https://doi.org/10.2514/1.16798.

[6] Holzäpfel F., Steen M., 2007: Aircraft Wake-Vortex Evolution in Ground Proximity: Analysis and Parameterization, AIAA Journal, Vol. 45, No. 1, pp. 218-227, https://doi.org/10.2514/1.23917.

[7] Sölch, I., Holzäpfel, F., Abdelmoula, F., Vechtel, D., "Performance of on-board wake vortex prediction systems employing various meteorological data sources", J. Aircraft, Vol. 53, Issue 5, pp. 1505-1516, 2016, DOI: : http://arc.aiaa.org/doi/abs/10.2514/1.C033732.

[8] Holzäpfel, F., "Effects of Environmental and Aircraft Parameters on Wake Vortex Behavior," Journal of Aircraft, Vol. 51, Issue 5, 2014, pp. 1490-1500, https://dx.doi.org/10.2514/1.C032366.

[9] ICAO, Manual on a 300 m (1 000 ft) Vertical Separation Minimum Between FL 290 and FL 410 Inclusive, International Civil Aviation Organization, Doc 9574, AN/934, 3rd edition, 62 pages, 2012.

[10] Crow, S.C., "Stability theory for a pair of trailing vortices," AIAA Journal, Vol. 8, 1970, pp. 2172–2179.

[11] Proctor, F. H., Hinton, D. A., Han, J., Schowalter, D. G., and Lin, Y.-L., "Two-Dimensional Wake Vortex Simulations in the Atmosphere: Preliminary Sensitivity Studies," AIAA Paper 97-0056, Jan. 1997.

[12] Delisi, D.P., Robins, R.E., "Effects of Crosswind Shear on Trailing Vortex Evolution," AIAA Paper 2006-1075, 44th AIAA Aerospace Sciences Meeting and Exhibit, 2006, Reno, Nevada.

[13] Bauer, T., Vechtel, D., Abdelmoula, F., Immisch, T., "In-Flight Wake Encounter Prediction with the Wake Encounter Avoidance and Advisory System," AIAA Paper 2014-2333, 6th AIAA Atmospheric and Space Environments Conference, 2014.

[14] Delisi, D.P., Pruis, M.J., Wang, F.Y., Lai, D.Y., "Estimates of the Initial Vortex Separation Distance, bo, of Commercial Aircraft from Pulsed Lidar Data", AIAA Paper 2013-0365, 51st AIAA Aerospace Sciences Meeting, 2013, Grapevine, Texas.

[15] Brown, A.P., Bastian, M, Alavi, S., Wasey, M., "Flight Research Report: Projects AEAFFR, CAAFER AND NASA ACCESS II Jet Transport Emissions Measurements," LTR-FRL2015-0054, National Research Council Canada, March 2015.